Unchannelized collapse of wet granular columns in the pendular state: Dynamics and morphology scaling

Pingshan Li ⬤, Dengming Wang ⬤,* and Zhiyang Niu

Department of Mechanics and Engineering Science, School of Civil Engineering and Mechanics,
and Key Laboratory of Mechanics on Disaster and Environment in Western China,
Ministry of Education of China, Lanzhou University, Lanzhou 730000, China

The unchannelized collapse of wet granular columns in the pendular state is investigated experimentally. Three different collapse regimes are observed in experiments, which are significantly dependent on the particle size as well as the initial aspect ratio of the column, while the water content has a quantitative effect on final deposit morphology. A dimensionless number containing the particle size and the water content is proposed to quantitatively characterize the macroscopic cohesion induced by the presence of water. On this basis, a phase diagram is put forward for describing different collapse regimes of wet granular materials. Furthermore, the dynamics and the resulting deposit morphology after collapse are primarily examined based on a series of experiments, particularly in two typical collapse regimes, where the coupling effects of particle size, water content, and initial aspect ratio of the column are mainly considered. Finally, generalized scaling laws have been developed to characterize the dependency of the deposit morphology on two relevant variables: the initial aspect ratio and the proposed dimensionless parameter. The morphological quantities in the wet case may be determined by respectively adding the variations caused by the cohesion effect to the results of dry granular material. The proposed scaling laws can be well degraded to those obtained in dry granular material when the cohesive effect inside wet granular material is weak enough. This implies that generalized scaling laws can be applicable to the collapse of granular material in a wider range of situations.

I. INTRODUCTION

Gravity-driven mass movements, such as rock avalanches, debris flows, pyroclastic flows, and mineral transport, are particularly common in the geophysical field and engineering applications [1,2]. Such flows generally pose a significant threat to downstream buildings and facilities due to their high mobility as well as huge impact consequences. Mass flows are prevalent in geophysics and engineering situations that are extremely complicated, and their flow behaviors are heavily influenced by the surrounding medium (liquid or air). Understanding such complicated flows is challenging due to the vast variety of phenomena presented by the flows in various situations [3,4]. As a result, quantitative analysis of the flowing process from the perspective of granular material, based on some controllable small-scale laboratory experiments and numerical simulations [5–7], is beneficial for essentially understanding such complex flow phenomena and their occurrence mechanism.

Although much progress has been made in the description of cohesionless granular flows in various configurations, the flow of cohesive granular materials remains poorly understood. Cohesion, in

---

*dmwang@lzu.edu.cn

　　　　　　　084302-1

particular, affects the dynamics of granular materials, resulting in certain qualitatively unexpected behaviors. Cohesion arises from interparticle forces that may involve different physical processes, such as van der Waals forces in dry powders [8], solid bonding in rock fragmentation [9], polymer cohesion [10], and capillary bonding in wet sand [11]. Most of the studies are concerned with the dynamics of wet granular materials, where cohesion is primarily induced by a certain amount of interstitial liquid. The amount of liquid may result in a variety of wet granular material states, including pendular, funicular, capillary, and slurry states [12–14]. The study of granular materials with low liquid content, particularly in the pendular state, is critical due to their prevalence in nature and in industrial settings, as well as the fact that this regime can be caused by a variety of circumstance factors such as ambient humidity and rainfall. Because of the presence of a small amount of liquid, liquid bridges form separately at the contact locations of paired particles within wet granular material in the pendular state [15,16]. The building and breaking of liquid bridges have an effect on the capillary and viscous forces between particles, resulting in a bulk cohesion, which can dramatically change the strength and macroscopic mechanical behaviors of the granular media [17–19].

The majority of current research in this area focuses on the changes in the mechanical properties of granular media caused by small amounts of added water as the interstitial liquid, such as variations in the repose angle [20], pile stability [21], Coulomb cohesion [22], elastic shear modulus [23], tensile strength [24], and volume fraction [25]. Adding a small amount of liquid to granular material also has a considerable effect on its dynamics. The cohesion induced by the presence of liquid can not only promote the convective-diffusion motions of the particles and obtain better mixing dynamics [26], but it can also give rise to the changes in the internal microstructure of the system, which enhances the dilatation effect of flow [27]. Furthermore, as the liquid content increases, different flow regimes of wet particles were observed in a rotating drum apparatus [28], indicating that the liquid content is a key factor that can significantly affect the avalanche dynamics of wet granular media. According to DEM simulations, increasing liquid surface tension can cause the maximum angle of stability of wet granular flow in a rotating drum and also lead to the transition from a continuous surface flow to a discrete avalanche flow [29,30], demonstrating that the properties of the liquid also play an important role in determining the dynamics of wet granular material.

The collapse of a granular column is a typical configuration that can quantitatively reveal the transient dynamical behavior of granular material as well as clarify the rheological features involved in granular flow [31,32]. In this regard, the collapse of dry granular material has been extensively studied in axisymmetric [33,34] or quasi-two-dimensional rectangular channelized configurations [35,36], and some useful results were also obtained, primarily in terms of the dynamics of the collapsed material and the scaling laws proposed for describing the final deposit morphology after the collapse.

However, there are few studies in the case of wet granular materials, particularly those with low liquid content. Artoni *et al.* [37] experimentally investigated the collapse of the quasi-two-dimensional wet granular column in the pendular state, as well as the dependence of the final deposit morphology and the runout dynamics on the liquid amount and the Bond number. The effects of the small amounts of liquid on the flow dynamics as well as the internal mechanisms of collapse for wet initial conditions were quantitatively examined using experiments and discrete element method (DEM) simulations, taking into account the failure, formation, and redistribution of the liquid bridge [38], and comparing to the dry case in similar configurations. It has been concluded that the irregular shape of particles may give rise to an additional mechanism with surface wetting and liquid spreading on the particle surface that accounts for the runout distance and the final deposit profile observed in experiments for the collapse of a column composed of wet coarse sands [39]. Similarly, cohesive forces between the particles can generate the rough surface of a cohesive granular deposit, the size of which increases with the interparticle cohesion, and the profile exhibits a self-affine behavior [40]. It is worth noting that the particle size in these related studies is quite large; therefore the capillary effect between particles is relatively weak when compared to the particle weight. We recently tried to conduct a series of experiments with glass beads of a larger size range at a low saturation level that just corresponds to the pendular state, and observed three different

collapse regimes of a wet granular column [41], which mainly depend on the initial aspect ratio of the column and the particle size but are almost independent of the water content.

Despite these efforts, it remains unclear how a small amount of interstitial liquid affects transient dynamic behaviors of wet granular material. A dam-break collapsed configuration, in which the flow is commonly along a specific two-dimensional channel, has accounted for the majority of its dynamical behaviors. However, previous studies have shown that the friction caused by the sidewalls has a significant effect on the dynamics of the collapse in this configuration [42,43]. As a result, the presence of sidewalls has a certain effect on the collapse dynamics of the granular column as well as the final deposit morphology, which may be more prominent in the wet granular case. Furthermore, it is still unclear how the dynamics in the granular collapse reacts to the presence of liquid in an unchannelized configuration more representative of actual situations, and whether there is a generalized scaling law characterizing the deposit morphology of wet granular columns in this configuration, just as there is for dry particles. The goal of this study is to systematically investigate the unchannelized collapse of wet granular columns in the pendular state, where the friction effect of sidewalls is purposely avoided. The research primarily focuses on the collapse dynamics and final deposit morphology of wet granular material, with a special emphasis on the development of generalized scaling laws by introducing several determining factors such as the initial aspect ratio of the column, particle size, and water content.

The paper is organized as follows. The experimental setup and measurement technique are described in Sec. II. In Sec. III, three different collapse regimes are experimentally observed and the corresponding phase diagram is proposed. The dynamics of the collapse and the deposit morphology are also included in this section. The effect of water content on the deposit morphology is discussed exclusively in Sec. IV. In Sec. V, the generalized scaling laws are proposed to characterize the deposit morphology of wet granular collapse in this configuration. Finally, in Sec. VI, our conclusions are summarized.

II. EXPERIMENTAL DETAILS

A. Experimental setup

The experimental setup for the unchannelized collapse of a wet granular column in the pendular state is sketched in Fig. 1, which primarily consists of a rectangular Plexiglas box with a length of 5 cm, a height of 80 cm, and a width of 10 cm. The front panel of the box remains transparent to allow a high-speed camera to capture images from the front, while the back wall is covered with black wallpaper to improve light contrast [36]. A smooth aluminum baffle serving as a retaining wall is vertically positioned at the right end of the box, delimiting a reservoir for maintaining a granular column in which wet particles can be filled before being released. For ensuring a horizontally rough base plane onto which the granular column was released, a glass plate of length $L_b = 100$ cm and width $W_b = 100$ cm is covered with sandpaper of roughness of 250 μm on its top surface and extended uniformly as the bottom of the box. The collapse of a granular column is initiated by quickly removing the baffle to release the particles that radially spread out on the horizontal plane under the gravity until they come to rest as a granular pile with diverse deposit morphologies. In a dam-break experiment, the velocity of the baffle removal is an important factor that should be considered [44]. Although the removal of the baffle inevitably perturbs the particles in its vicinity, it has been demonstrated that the movement of the baffle has a negligible effect on the collapse dynamics if the average release velocity of the baffle is more than $0.4\sqrt{gH_i}$ [45]. In our experiments, the velocity of the baffle removal can be estimated using the high-speed camera, and it is at least 1.2 m/s, which is substantially higher than the critical velocity proposed in the above experiment. Furthermore, for wet granular materials, the existence of cohesion may further weaken the possible effect of the initial perturbation on the collapse process. Therefore, the effect of the removal velocity of the baffle on the collapse of wet granular columns may be negligible in our experiments.

The initial aspect ratio of the column a, commonly defined as the ratio of its initial height H_i to length L_i, can be varied from 0.3 to 15.0 by adjusting the height H_i while keeping its length $L_i = 5.0$ cm. Glass beads of density $\rho_g = 2510$ kg/m^3 with four different mean diameters
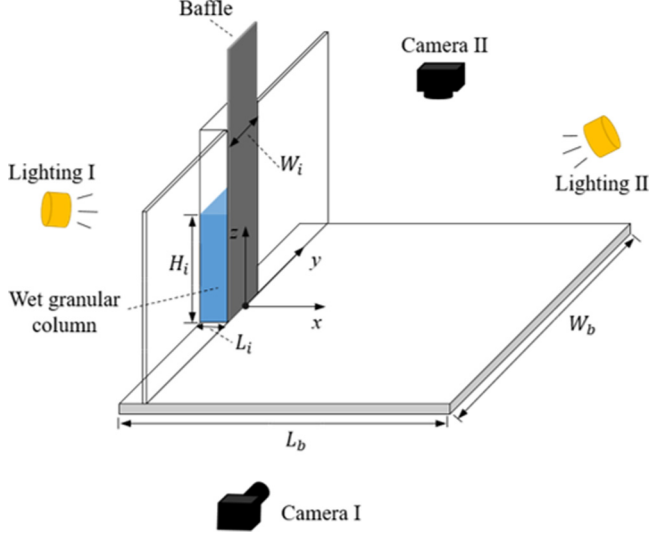
FIG. 1. Schematic diagram of the experimental setup for the unchannelized collapse of wet granular columns in the pendular state.

$d = 0.5 \pm 0.05$ mm, 1 ± 0.1 mm, 2 ± 0.1 mm, and 5 ± 0.2 mm are used for the experiments, whose size can be reliably quantified using a Microtrac S3500 laser particle size analyzer. The wet particle sample is prepared by adding pure water of mass m_w with a surface tension of 74 mN m^{-1} as the interstitial liquid to dry glass beads of mass m_p in a rotating drum, and then rotating at a certain speed for a long enough period to ensure that the two types of materials are well mixed. The sample prepared using this procedure is proved to be sufficiently homogenous by an x-ray tomography scanner [37,39]. Based on a capillary model at contact proposed by Johnson *et al.* [10], the capillary force between wet particles in our experiments can be estimated to be in the range of 0.17–1.74 mN, whose values are comparable to the results of Richefeu *et al.* [22]. The prepared sample is poured into the reservoir using a funnel, forming a wet granular column. It should be noted that there is water loss induced by the amount of loss left on the inner wall of the drum as well as the amount of water evaporation during the sample generating process of a wet granular column. Even though the amount of water involved is minimal, the additional compensating water is also added to the mixture before release to ensure that the water content in the experiments is accurate, which is based on the estimated value of water loss based on the calibration experiments [39,46].

As a result, the water content within the wet granular material can be quantitatively characterized by the mass percentage of water $w = m_w/m_p \times 100\%$ [37], where m_w contains the amount of compensatory water as discussed above. In our experiments, we employ the granular samples with a variety of water contents, mainly including $w = 0$(dry), 0.5%, 1%, 2%, and 4%, whose value always ensures wet glass beads at a low saturation level that just corresponds to the pendular state [22,26]. To acquire reproducible results, each set of tests will be repeated 3 to 5 times.

B. Measurement technique

In each experiment, the collapse of the granular column is recorded at regular intervals by two high-resolution high-speed cameras (IDT NR4S1), positioned to the side and above the area where the column collapses to catch the entire flow process from two different directions. The tests are carried out in a dark environment, which can effectively improve light contrast and reduce external optical contamination. The horizontal base plane of the experimental setup is covered with black sandpaper, with a black background wall placed behind it to capture the high-definition images from

the side view. Both cameras are connected to a central computer, enabling synchronous shooting as well as data transfer at any time to record the long-lasting experimental process. The frame rate of the high-speed camera is up to 500 fps (frame per second) and the size of the captured window can be adjusted by its relative position, allowing it to capture an area of interest with a resolution of 1280×1024 pixels for each image. The deposit morphology of collapsing material, such as the height profile and the pileup boundary on the horizontal surface, can be easily extracted at each time step by analyzing image sequences. The data obtained can be used to explore the dynamics and evolving features of the collapsed material.

The particle image velocimetry (PIV) technique is applied to investigate the evolution of the velocity field. It works by computing the cross-correlation function of the image intensity field between two consecutive images recorded within a short time interval. Each image was divided into rectangular regions called interrogation windows, and the algorithm was usually implemented using multiple channels and deformation windows of the fast Fourier transform (FFT). We employed three channels with different interrogation windows with the sizes of 64, 32, and 16 pixels in both dimensions, respectively. The step size of each channel, i.e., the spacing between the centers of the interrogation area, is half the size of each interrogation area. The spline interpolation was used to acquire the displacement at each pixel of the interrogation area, while the Gaussian interpolation was used for the subpixel estimation [47]. Due to the cohesion induced by the presence of water in our experiments, a few particles remained attached to the sidewall or the baffle after the collapse. This is an unavoidable phenomenon in wet granular experiments [37], but it does not affect the measurement results.

III. UNCHANNELIZED COLLAPSE OF WET GRANULAR MATERIAL

The collapse process of wet glass beads was continuously recorded using two synchronized high-speed cameras from two different directions. Qualitative observations revealed that the dynamics of collapsing material and its final deposit morphology significantly depended on the particle size d, the column's initial aspect ratio a, and the water content w. Three different collapse regimes were distinctly observed in the experiments.

A. Different collapse regimes

To begin, we will investigate how the particle size d affects the unchannelized collapse of a wet granular column. When $a = 3$ and $w = 1\%$, five consecutive images on the collapsing process of the columns made of wet glass beads of two typical mean diameters are shown in Fig. 2. The result in the dry situation is also provided for comparison. The evolving features of the deposit morphology after the collapse are observed synchronously from two different viewing directions. Only the deposit on the horizontal surface is shown in the top view, and the in-plane size is proportionally scaled down to be completely displayed.

Figure 2(a) shows the collapse process of a dry granular column in the unchannelized dam-break configuration. From the side view, the collapse exhibits some typical characteristics similar to those observed in channelized collapse flows [31,35]. The upper part of the column undergoes a vertical free-fall motion due to gravity at the initial stage of the collapse. After reaching the vicinity of the stationary region, the toe of the collapsing material gradually develops into a flow front that continuously propagates along the longitudinal direction, and the moving particles flow over a gradually inclined stationary deposit. As a result of the collapse, the granular mass spreads out on a horizontal surface and eventually forms a heap. The lateral spreading flow plays an important role in determining the dynamics of the collapsing material and its final deposit in this configuration, as seen from the top view. Due to the absence of sidewalls, the margin of the free-falling column promotes the development of lateral motions under the action of gravity, and small cascades are developed to adjust the slope of the growing stationary deposit toward an equilibrium state. The moving particles progressively evolve into a bulk surface flow that spreads out along the radial direction until it forms a rounded deposit on the horizontal surface, which is comparable with the
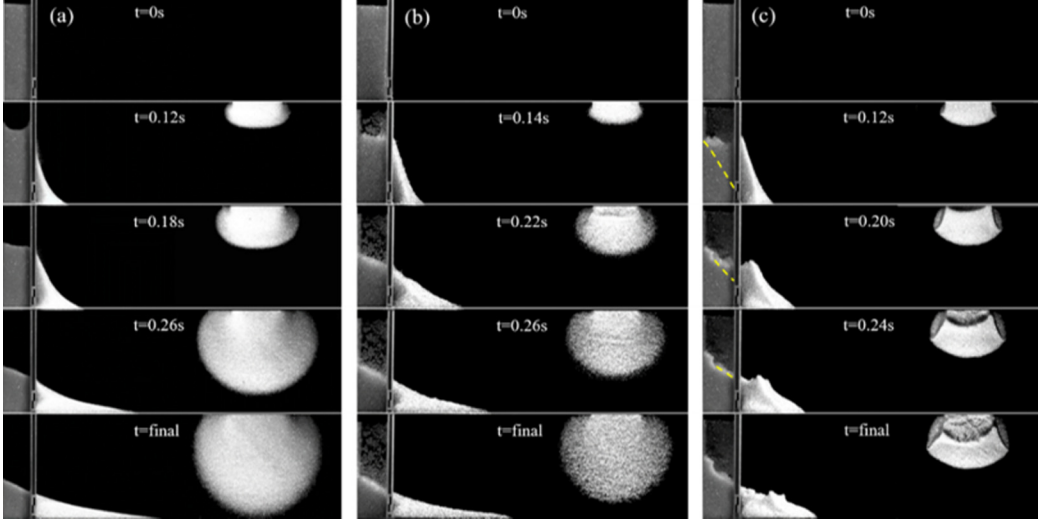
FIG. 2. Snapshots of the evolution of the collapse flow of granular columns with various particle sizes at an initial aspect ratio of $a = 3$. (a) $d = 0.5$ mm, $w = 0\%$, (b) $d = 2.0$ mm, $w = 1\%$, and (c) $d = 0.5$ mm, $w = 1\%$. The yellow dashed line in (c) represents the failure plane obtained from the velocity field in the side view.

results obtained from a DEM simulation of dry granular material in a similar configuration [43]. It should be noted that the collapse of dry granular material appears to be almost independent of the particle size; hence we only provide the data for $d = 0.5$ mm.

However, if a granular material is mixed with a certain amount of water, the liquid-induced cohesion enables the collapse of wet granular columns to exhibit a clear dependency on the particle size, as seen in Fig. 2. When the particle size is large enough (e.g., $d = 2.0$ mm), the cohesion between the particles is weak enough in comparison to the particle's weight that the particle flow is primarily driven by gravity. As a result, the collapse of wet granular material resembles the collapse of dry particles in certain ways, including the spreading of the flow front and the deposit morphology as well [Fig. 2(b)], which is referred to as the continuous collapse (CC) regime in our experiment. In comparison to the dry case, the presence of water causes some quantitative changes in the collapse, such as the deposit having a shorter runout distance as well as a larger final maximal height, which will be detailed in the next section.

When the particle size is small (e.g., $d = 0.5$ mm), the collapse of a wet granular column exhibits some characteristics different from those observed in a dry granular system, as shown in Fig. 2(c). In this case, the motion of the particle is dominated by the interparticle cohesion, where the capillary force between the particles, estimated by a capillary model proposed by Johnson *et al.* [10], exceeds 10 times the weight of the particles. The flow is initiated by the shear failure along with the interface between the flowing and stationary layers, depicted using the yellow dashed lines in the side view. The part of the column above this failure plane slides to the right front as a whole, and the initial shape of the free surface of its right-upper corner remains almost unchanged at the beginning of the collapse. During the subsequent sliding process, the toe of this slide body will develop into a flow front on the horizontal surface, while its upper part gradually deforms or even fractures, eventually forming a nearly fan-shaped irregular deposit pile. The final deposit has a rough blocklike surface, and exhibits a distinct peak structure as seen from the top view, where the peak lines are correspondingly evolved from the prismatic edges of the column in contact with the baffle before the collapse. In our experiment, the collapse with such features is referred to as the block collapse (BC) regime. In this regime, the deposit commonly has a nearly wedge-shaped morphology with a nonmonotonic, uneven height profile from the side view.
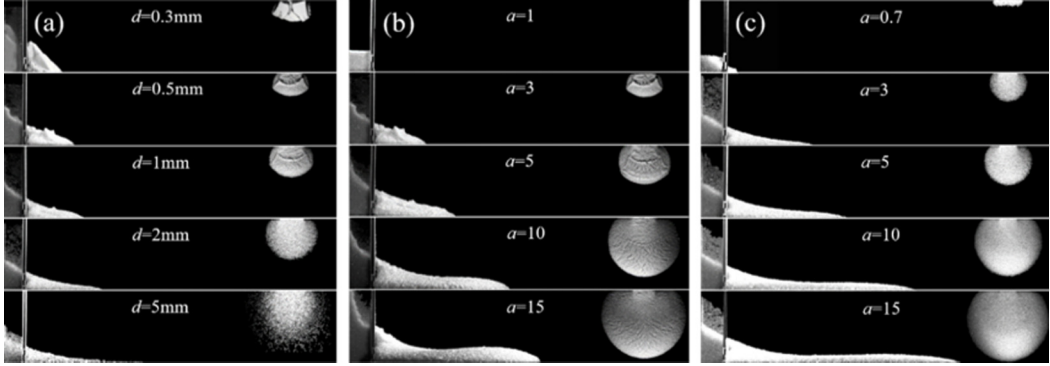
FIG. 3. Final deposit morphology of the collapsed wet granular column under different experimental conditions. (a) Different d at $a = 3$, (b) different a for $d = 0.5$ mm, and (c) different a for $d = 2.0$ mm. The water content $w = 1\%$.

Overall, the particle diameter d plays a crucial role in the dynamics of the collapse and the resulting deposit of wet granular material in the pendular state, which may essentially lead to a change in the relative magnitude of the cohesive force between interparticles and the particle's weight. To address this further, we present the final deposit morphology of a wet granular column by altering only the particle size while holding all other parameters constant, as shown in Fig. 3(a). As the particle diameter increases, the surface blocks on the deposit, which are comparable in size to the column's initial height at $d = 0.3$ mm, may gradually shrink to the particle-scale roughness. Accompanied by the transition of the collapse regime, the deposit on the horizontal surface evolves from an irregular to a nearly rounded region observed from above, and its height profile accordingly changes from a nonmonotonic and uneven to a continuous monotonic curve. Although it can be recognized by the deposit morphology that the collapse in the case of $d = 5.0$ mm belongs to the CC regime, the deposit extent is quite blurred as some particles are detached from the main deposit pile and scattered farther, a phenomenon that has also been observed in similar dry particle collapse [43,48].

In addition to the particle size, the initial aspect ratio of column a also plays an important role in the collapse of the wet granular column. We further present the deposit morphology after the collapse of a wet granular column with various aspect ratios a at two typical particle sizes d, as shown in Figs. 3(b) and 3(c). Since the macroscopic cohesion induced by the presence of water overcomes the weight of the particle, the short column (e.g., $a = 1$) composed of wet glass beads remains in its initial configuration without collapse for a long period in the case of $d = 0.5$ mm, which is referred to as the noncollapsed (NC) regime in our experiment. With the increase of a, the column begins to collapse under gravity. Particles aggregate on the surface of the deposit, leading to the roughness on the macroscopic scale. Although such a rough surface featured with superficial blocks gradually weakens with increasing a, its height profile still exhibits an uneven feature in the local segment even though a is large enough (e.g., $a = 15$), which is regarded as the BC regime as well. As a result, for a wet granular column composed of particles of $d = 0.5$ mm, the increase of a leads to a transition from the NC to BC regimes. Furthermore, in the case of $d = 2.0$ mm, the collapse of the wet granular column also undergoes a transition from the BC to CC regimes with the increase of a, as shown in Fig. 3(c). If the column is short (e.g., $a = 0.7$), the uneven height profile can be distinctly observed from the side, even though it is difficult to recognize from the top view. When a is large (e.g., $a \geqslant 1.0$), the height profile of the deposit is approximately monotonic and continuous, and the deposit on the horizontal surface has a nearly rounded region, after which the collapse transforms to the CC regime.

B. Phase diagram

According to our observations, in the unchannelized configuration, a wet granular column exhibits three different collapse regimes, which are primarily determined by the particle size d and the initial aspect ratio a in the experiments. Although the water content w has no substantial influence on the collapse regime, as previously demonstrated in the channelized collapse experiment [41], it does have a quantitative effect on the deposit morphology of wet granular materials, including the runout distance and deposit height. More crucially, the effect of w on the dynamics of wet granular material is commonly coupled with the particle size [37]. As a result, we attempt to characterize the dependence of wet granular collapse on two relevant factors in our experiments. The first is the initial energy of the column, which is proportional to the initial aspect ratio a. The other kind is the bulk cohesion induced by the presence of a small amount of water. To quantitatively characterize such a macroscopic cohesion effect within wet granular material, we use a dimensionless number $B_o^{-1}w^{2/3}$ introduced by Artoni *et al.* [37], where $B_o = \rho g d^2 / \gamma$ is the ratio of the particle's weight to the capillary force, and γ is the surface tension of the liquid.

To accurately identify the collapse regime, a quantitative approach is used based on the analysis of the surface roughness of the deposit morphology in the side view [40], especially for the cases where the morphological features of the deposit are not sufficiently prominent. We define the difference function based on two height profiles as follows,

$$\eta(x) = h(x) - \bar{h}(x), \tag{1}$$

where $h(x)$ is the height profile of the final deposit, and $\bar{h}(x)$ is the corresponding monotonic fitted profile. The function $\eta(x)$ exhibits certain fluctuations around zero along the x direction, and the fluctuation height may increase when the cohesion effect triggers the free surface of the deposit to show distinct blocklike features. Accordingly, the typical length l_z of the fluctuation in the z direction can be defined through the standard deviation of its difference distribution along the x direction,

$$l_z = \sqrt{\langle \eta^2 \rangle_x - \langle \eta \rangle_x^2}, \tag{2}$$

where $\langle \cdots \rangle_x$ denotes the average over the coordinate x. Based on such a definition, l_z can be used to quantitatively characterize the surface roughness of the deposit morphology. Combined with the qualitative determination of the surface morphology of the deposit in the top view, a critical height of the fluctuations, i.e., $l_z^c \approx 0.8 d_0$ with $d_0 = 1.0$ mm, is proposed to quantitatively distinguish wet granular collapse between the BC and CC regimes in our experiments.

Based on this quantitative identification approach as well as the experimental data under various conditions, we propose a phase diagram in the phase space of $B_o^{-1}w^{2/3}$ and a to describe different collapse regimes of a wet granular column in an unchannelized configuration, as shown in Fig. 4.

From the figure, it can be seen that when the dimensionless number $B_o^{-1}w^{2/3}$ is small, corresponding to the cohesion effect in the granular system being relatively weak, the collapse of the wet granular column behaves as the CC regime. As this dimensionless number increases, the collapse progressively evolves into a BC regime, and it even enters the NC regime for short columns (e.g., $a \leqslant 1$ here), which is attributed to the increase in the macroscopic cohesion of the system. On the other hand, the increase in a also can give rise to the transition between different collapse regimes, which seems to be dependent on the magnitude of $B_o^{-1}w^{2/3}$. This is primarily owing to the large initial potential energy, which allows it to overcome the cohesion within wet granular material during the collapse. The transition between different collapse regimes has been discussed in detail in our previous work on the channelized collapse of wet granular material [41], which appears to have a mechanism similar to that of the current experiment and hence will not be further discussed in this paper.
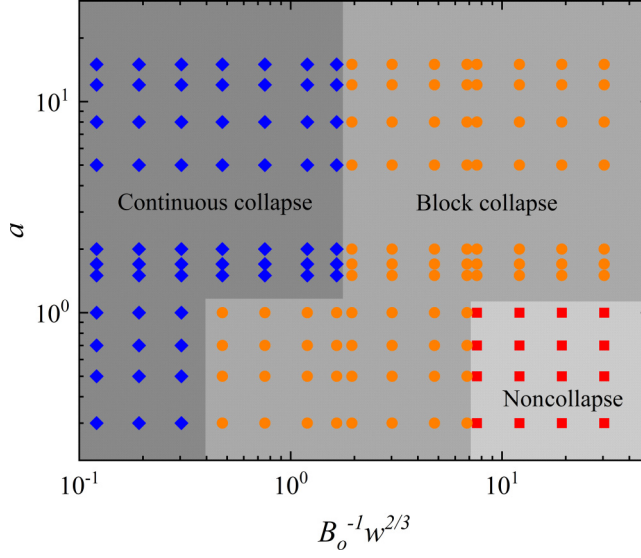
FIG. 4. Phase diagrams in phase space ($B_o^{-1}w^{2/3}$, a) for describing the collapse regimes of wet granular material, where red squares (■), light blue circles (●), and dark blue diamonds (◆) correspond to the noncollapse (NC), block collapse (BC), and continuous collapse (CC) regimes, respectively.

C. Dynamics of collapse

In this section, we analyze the collapse dynamics of a wet granular column and discuss its dependence on particle size, particularly in two different collapse regimes. The radial spreading of the flow front determines the collapse dynamics and the resulting final deposit in the unchannelized configuration. We first plot the longitudinal distance L and the lateral width W of the spreading material with time for a wet granular column with $a = 3$, as shown in Fig. 5, where the distances along two directions are normalized by the initial length L_i and width W_i of the column, respectively,
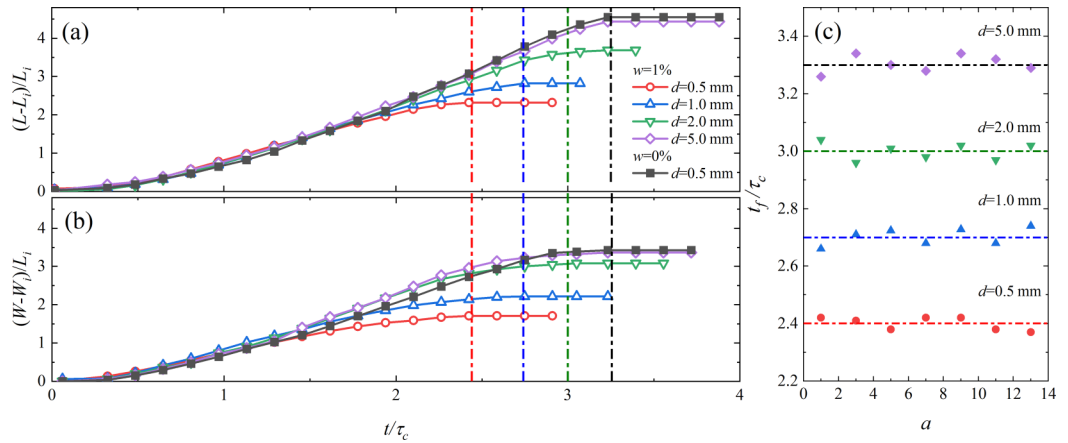

FIG. 5. Scaled spreading distance on the horizontal surface traveled by the flow front as a function of normalized time in the unchannelized collapse of wet granular materials with different particle sizes at $a = 3$. (a) The length along the longitudinal direction. (b) The maximum width along the lateral direction. The dashed lines in different colors correspond to the duration of wet granular flow for different particle sizes, respectively. (c) The variation of normalized flow duration t_f/τ_c with the initial aspect ratio a for different particle sizes.
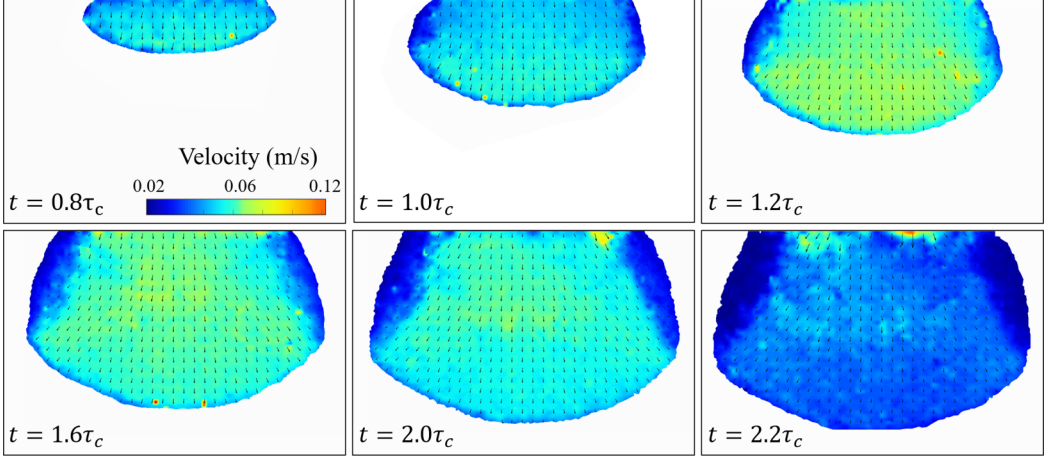
FIG. 6. Velocity field at successive time steps in the BC regime, where the water content $w = 1\%$, the particle diameter $d = 0.5$ mm, and the initial aspect ratio of the column $a = 3$. The colors and arrows in the velocity field are used to visualize the magnitude and direction of the velocity in the collapse flow, respectively.

and time is normalized by the free-fall characteristic time $\tau_c = \sqrt{H_i/g}$. We also show the results of dry particles under the same conditions for comparison.

In this configuration, the flows in both longitudinal and lateral directions appear to be spreading synchronously, as seen in Figs. 5(a) and 5(b). The whole flow process of wet granular material consists of three typical stages: initial acceleration, the intermediate constant velocity, and ultimate deceleration, which is quite similar to the phenomenon in the dry case. The normalized flow duration of the dry particles in this configuration, as shown in Fig. 5, is around $3.3\tau_c$ in both directions, regardless of the particle size, which is consistent with the result obtained in a channelized collapse of dry granular material [32]. However, for the unchannelized collapse of a wet granular column, the normalized duration is reliant on the particle size, although remaining almost constant in both directions and being almost independent of the initial aspect ratio. For particles with small sizes, the flow duration is shorter than the result of dry particles, as shown by the dashed lines in different colors in Fig. 5, which is primarily due to the shortening of the constant-velocity stage. The duration of wet granular collapse gradually increases with the particle size, and finally converges to the result of dry material when d is large enough (i.e., $d = 5.0$ mm). We also present the variation of normalized flow duration t_f/τ_c with the initial aspect ratio a for different particle sizes, as shown in Fig. 5(c). It can be seen that the normalized duration of wet granular material is almost independent of the initial aspect ratio a, which is consistent with the observations for dry particles in the channelized collapse [36,49].

Based on the foregoing findings, the position evolution of the flow front along two mutually perpendicular directions does not appear to reveal substantial differences in the two collapse regimes. To better understand the formation mechanism of different deposit morphologies, we further display the velocity field of spreading flow on the horizontal surface and analyze its evolving features throughout the collapse using the PIV technique. The ensuing series of sequential images for the top view vividly illustrates the progressive velocity vectors.

Figure 6 shows the velocity fields measured at successive time steps in the BC regime. At the beginning of the flow, the collapsed wet material rapidly develops a flow front that propagates along the longitudinal direction and maintains a specific shape with no visible lateral flow. During the flow process, the edge particles experience some local avalanches under gravity and are gradually deposited on both sides of the fan-shaped spreading zone, which can be observed from local regions on both sides of the velocity field where the velocity approaches zero, as shown in Fig. 6. Due
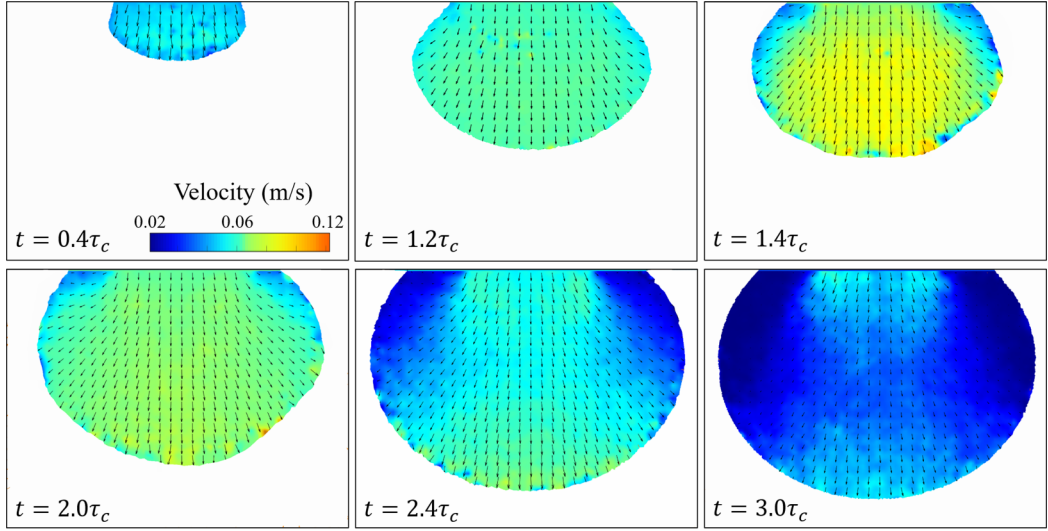
FIG. 7. Velocity field at successive time steps in the CC regime, where the water content $w = 1\%$, the particle diameter $d = 2.0$ mm, and the initial aspect ratio of the column $a = 3$.

to the high cohesion effect within the system, the lateral flow is not fully developed during the spreading stage, and the main flow area seems to suffer an overall deformation. As a result, as seen in the experiment, an irregular deposit resembling a roughly fan-shaped zone eventually forms on the horizontal base plane.

However, the velocity field exhibits completely different evolving features in the CC regime, as shown in Fig. 7. Because of the development of lateral motions from the beginning of the flow, the collapsing material forms a more elongated deposit cone with its long axis along the lateral direction. The free surface subsequently begins to flow, forming a flow front that propagates longitudinally and laterally. The margins of small cascades extend outward at this time, and the spreading flow appears to develop freely along the radial direction under the action of gravity, gradually altering the slopes of the growing deposit heap. As a result, the velocity field has a more uniform velocity distribution in the radial direction, comparable to what has been reported in simulations of dry particles under similar conditions [43]. The collapsing material continues to propagate along the free surface from the core toward the frontal region in the latter stage of the flow, eventually forming a spread-out cone with a rounded shape as seen in the top row.

D. Deposit morphology

The features characterizing its resulting three-dimensional deposit morphology are quantitatively analyzed from the side and top views, for the unchannelized collapse of a wet granular column in the pendular state. The height profile of the final deposit for various aspect ratios is presented at two particle sizes, as shown in Fig. 8, which respectively correspond to two different collapse regimes. The results in the dry case are also provided under the same conditions for comparison. It is worth noting that the height profile is defined as the contour of the maximum height of the final deposit along the longitudinal direction after the collapse, and it can be determined directly in our experiment by identifying the highest point of the quasi-2D deposit morphology from the side view.

Compared to the case of dry granular material, the addition of a small amount of water has a significant effect on the height profile of the deposit, and this effect is quite different under the two collapse regimes. In the BC regime, the presence of water leads to discontinuous and nonmonotonic height profiles of deposit heaps even though such unsmoothness gradually decreases with increasing
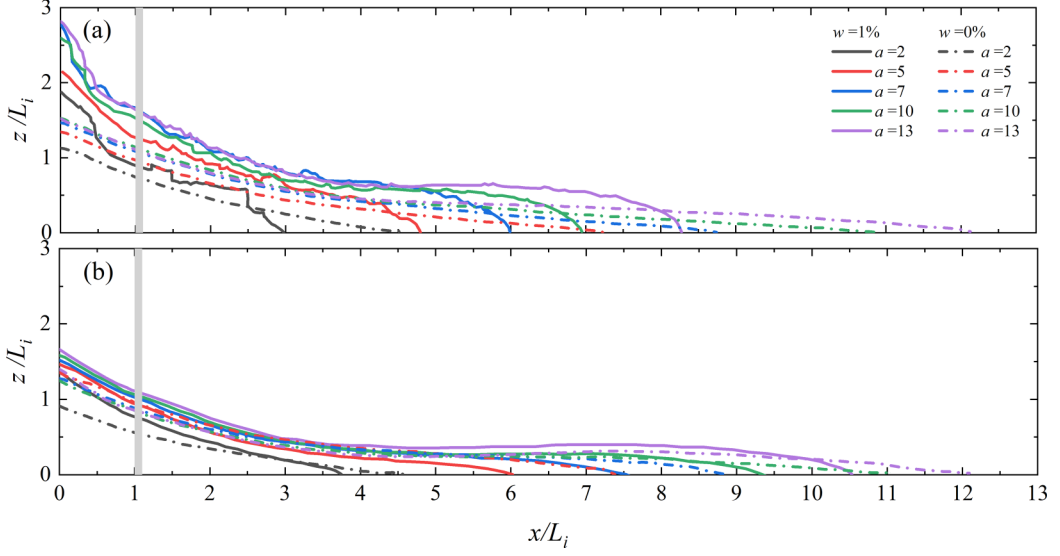
FIG. 8. The height profile of final deposit morphology after the collapse of a wet granular column for various a for the dry and wet cases. (a) Series of experiments in the BC regime with $d = 0.5$ mm; (b) series of experiments in the CC regime with $d = 2.0$ mm.

a, which is qualitatively different from the results of dry particles. For the CC regime, although the height profile exhibits some characteristics that resemble the dry case [43,48], there are some quantitative differences between the two cases. The deposit has a shorter runout distance as well as a higher maximum height in the wet case. Moreover, the top angle and the toe angle of the deposit heap both increase significantly when water is added to the material, though only a slight dependence is found on the aspect ratio a. Furthermore, from the side view, the height profile is qualitatively similar to the observations of a dam-break collapse of wet granular material [41], but there are some quantitative discrepancies. In the BC regime, under the same initial conditions, the height profile of the deposit displays a relatively weak unevenness in the unchannelized collapse. Since the lateral flow is not restricted, there is a slight drop in the height profile, including the heap slope, the runout distance, and the maximum deposit height, compared to the channelized case [39,41].

To better understand the differences in deposit morphology of wet granular columns in two collapse regimes and in comparison to dry granular collapse in the same configuration, we extracted the final deposit region on the horizontal base plane for two different particle sizes in the dry and wet situations and presented its horizontal deposit shape, as shown in Fig. 9, where the results for four different values of a are provided accordingly to highlight the role of the initial aspect ratio. Here the horizontal deposit shape is intuitively characterized using the edge contour of the final deposit pile on the horizontal surface measured from the reservoir outlet, which can be determined by identifying the radially spreading distance of the deposit from the top view.

The initial aspect ratio of the column and the presence of water both have a significant effect on the deposit morphology on the horizontal surface, as seen in the panels in the top row. When a dry short column (i.e., $a = 1.5$) collapses, it forms a deposit with a lateral extension greater than the longitudinal runout distance, which is almost independent of the particle size and agrees well with recent simulations [43]. In the wet condition, however, lateral spreading after the collapse of a short column is not fully developed due to the cohesion effect. The deposit has a smaller extent in this scenario, and its contour is an irregular shape that differs significantly from a circle of the same area. This feature is more prominent in the BC regime and shows a clear dependence on particle size.
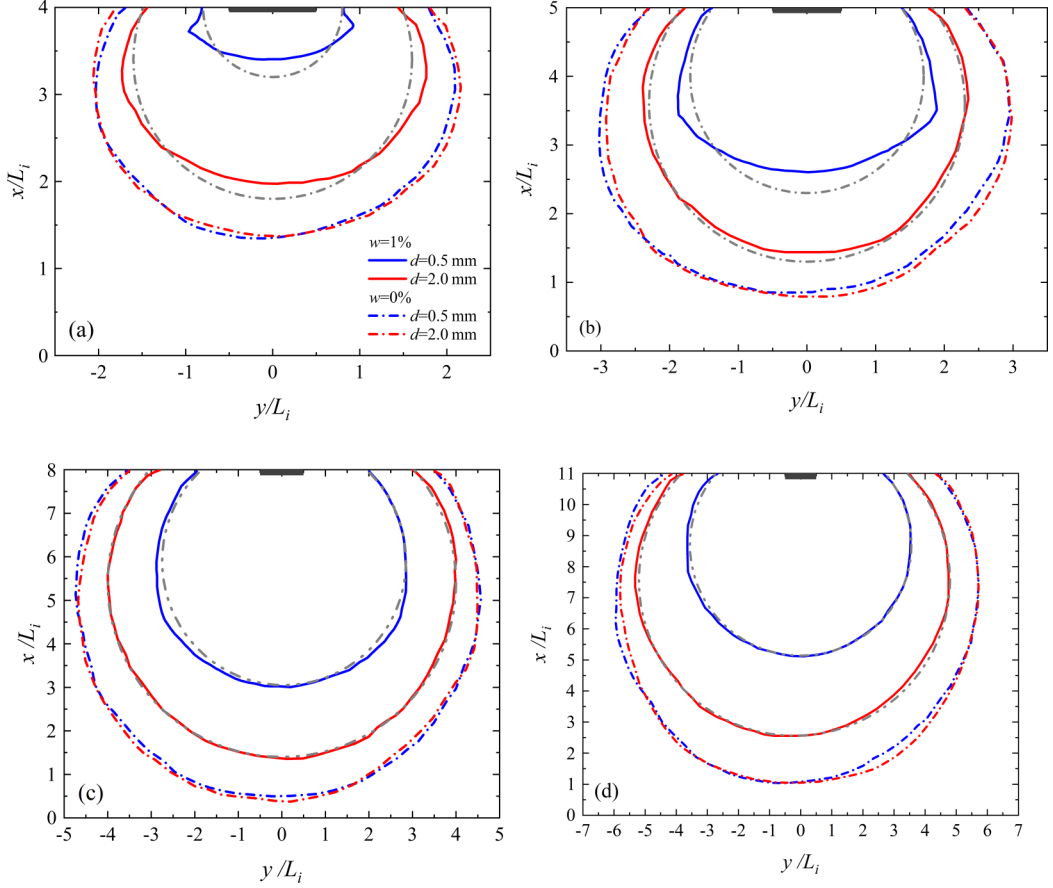
FIG. 9. The deposit shape on the horizontal surface after the unchannelized collapse of wet granular columns with different initial aspect ratios (a) $a = 1.5$, (b) $a = 3$, (c) $a = 7$, and (d) $a = 10$. The water content $w = 1\%$. The blue and red solid lines are the results of the particle size $d = 0.5$ mm and $d = 2.0$ mm, respectively, and the gray dashed line is the corresponding circle with the same area for comparison.

As the initial aspect ratio a increases, the lateral spreading of the collapsing material develops progressively. For larger particles, such development is more sufficient due to the liquid having a smaller influence on the dynamics of the collapse. As a result, a rounded deposit forms on the horizontal surface, comparable to the results for dry particles under the same conditions, even though the deposit extent is far smaller. On the other hand, the deposit of a wet granular column composed of small particles still forms an irregular fan-shaped zone on the horizontal surface, as shown in Fig. 9(b). When a is large enough (i.e., $a = 10$), the lateral flow of collapsing material has been fully developed, even in the case of wet particles with small sizes. Since the deposit on the horizontal surface is mostly determined by the radially spreading motions of the underlying particles, in this case, it will eventually develop into a circular region even though the collapse is still in the BC regime (Fig. 3). Based on our experimental observations, the critical value of the initial aspect ratio in the wet case, which corresponds to the deposit having just formed into a nearly rounded shape on the horizontal surface, must be greater than $a = 10$ for small particles, but only $a = 4$ at larger particles. The latter is nearly identical to the value for dry particles.
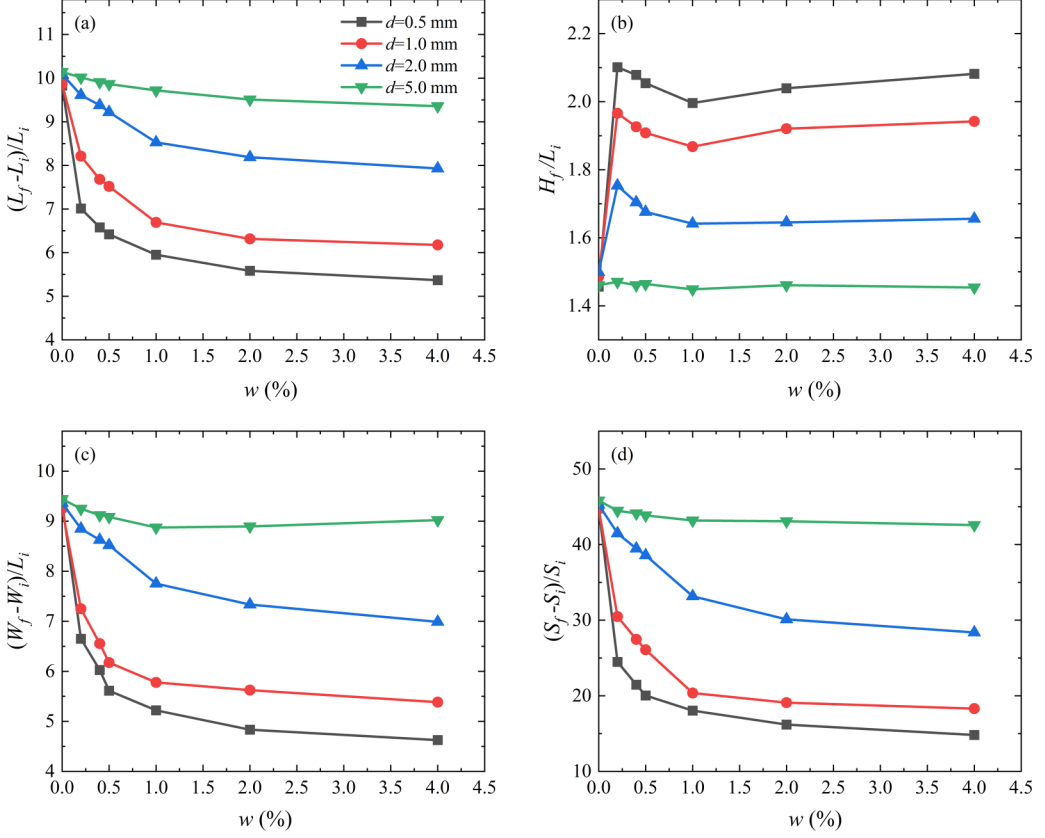
FIG. 10. The dependences of the runout distance (a), the deposit height (b), the deposit width (c), and the deposit area (d) on the water content for various particle sizes at the initial aspect ratio of the column $a = 10$.

IV. EFFECT OF WATER CONTENT ON THE DEPOSIT

According to our findings, while the water content has no significant effect on the collapse regime of wet granular material in the pendular state, it can have a quantitative effect on the deposit morphology, which may differ for particles of various sizes [37–39]. To investigate the role of water content in the unchannelized collapse of wet granular columns, we propose a set of parameters to quantitatively describe the deposit and further explore the impact of water content on them. The final deposit morphology is characterized by the runout distance ($L_f - L_i$), deposit height H_f, deposit width ($W_f - W_i$) measured from the deposition edges, and deposit area ($S_f - S_i$) on the horizontal surface, which all can be measured directly from the top and side views of the final deposit. The length quantities are all normalized by the column's initial length, while the deposit area is normalized by the column's base area. The coupling effect will be studied based on the results of different particle sizes because the cohesion caused by the presence of water is frequently related to the particle size. For four different particle diameters, the fluctuations of these normalized characteristic quantities with the water content w are shown in Fig. 10, where the initial aspect ratio of the column is $a = 10$.

From the above figure, it can be seen that the final runout distance, the deposit height, and the deposit area all decrease slightly as the water content increases, while the deposit height slightly increases, and a plateau period is nearly reached for all quantities when $w > 1\%$, and this dependence is present for different particle sizes and is well consistent with the results in the

channelized configuration [37,39]. On the other hand, the influence of water content on deposit morphology varies quantitatively depending on the particle size. The runout distance of wet particles is much smaller than that of dry particles when the particle size is small (i.e., $d = 0.5$ mm), and it decreases significantly as w increases. When the particle size is large enough (i.e., $d = 5.0$ mm), the rescaled runout distance of wet particles gradually increases and almost reaches the result of dry particles, as shown in Fig. 10(a), whose value is almost independent of w. With varying the particle size, several other characteristic quantities, as shown in Figs. 10(b)–10(d), have similar dependencies on the water content. These results can be explained by the fact that the coupling effect induced by the particle size and the surface tension in wet particle materials causes a shift in the balance between the capillary force and the body force at the particle scale. For larger particles, the weight of the particle dominates its motion, whereas the interstitial liquid has less impact on the dynamics of the particle material. In this case, variations in the water content have no significant effect on these characteristic quantities of the deposit morphology.

Overall, the water content has a quantitative effect on the collapse of wet granular materials in the pendular state; however, this effect is more reflected in the coupling with other relevant factors such as the particle size and the initial aspect ratio. The coupling of these factors can have a greater influence on the dynamics and deposit morphology of wet granular material, as well as also changing its collapse regime qualitatively. As a result, such a coupling effect must be taken into account while studying the deposit morphology of wet granular material, particularly when developing scaling laws that are satisfied by the aforementioned characteristic quantities.

V. GENERALIZED SCALING LAWS OF DEPOSIT MORPHOLOGY

In previous numerical simulations and experiments on the collapse of dry granular columns in the channelized configurations, two key morphological quantities, the normalized runout distance $(L_f - L_i)/L_i$ and the deposit height H_f/L_i, are commonly used to characterize the final deposit morphology [49,50], both of which are primarily dependent on the initial aspect ratio of the column in this configuration. As a result, some scaling laws are proposed to specifically describe these dependence relationships under a variety of conditions [43,51]. However, for the unchannelized collapse of a wet granular column in the pendular state, the scaling laws characterizing its deposit morphology are still lacking since the factors affecting its dynamics are relatively numerous and coupled with each other. In addition to the water content and the initial aspect ratio of the column, the particle size plays a crucial role which is not the case with dry granular material. Furthermore, the collapsing particles undergo significant lateral spreading in the unchannelized configuration, resulting in the deposit with a distinctive three-dimensional morphology. In addition to the two morphological quantities mentioned above, we propose the normalized deposit width $(W_f - W_i)/L_i$ and area $(S_f - S_i)/S_i$ to characterize the deposit region on the horizontal surface, where W_f and S_f are maximum deposit width and deposit area, respectively. On this basis, we attempt to explore how these quantities characterizing the deposit morphology vary with the particle size d, the water content w, and the initial aspect ratio of the column a when the cohesion effect is taken into account. For this purpose, we first present the fluctuations of four morphological quantities with a for various w and d, as shown in Fig. 11.

We examine the dependences of normalized runout distance and deposit height of wet particles on the initial aspect ratio a, as shown in Figs. 11(a) and 11(b), whose trends still show the typical characteristics of a channelized collapse of the dry granular column. Based on the experimental data, we propose the scaling laws to describe these dependencies as follows,

$$\frac{L_f - L_i}{L_i} = \begin{cases} A_{L1}a^{\xi_L} & a \geqslant 3 \\ A_{L2}a & a < 3 \end{cases}, \tag{3}$$

$$\frac{H_f}{L_i} = \begin{cases} A_H a^{\xi_H} & a \geqslant 1 \\ a & a < 1 \end{cases}, \tag{4}$$
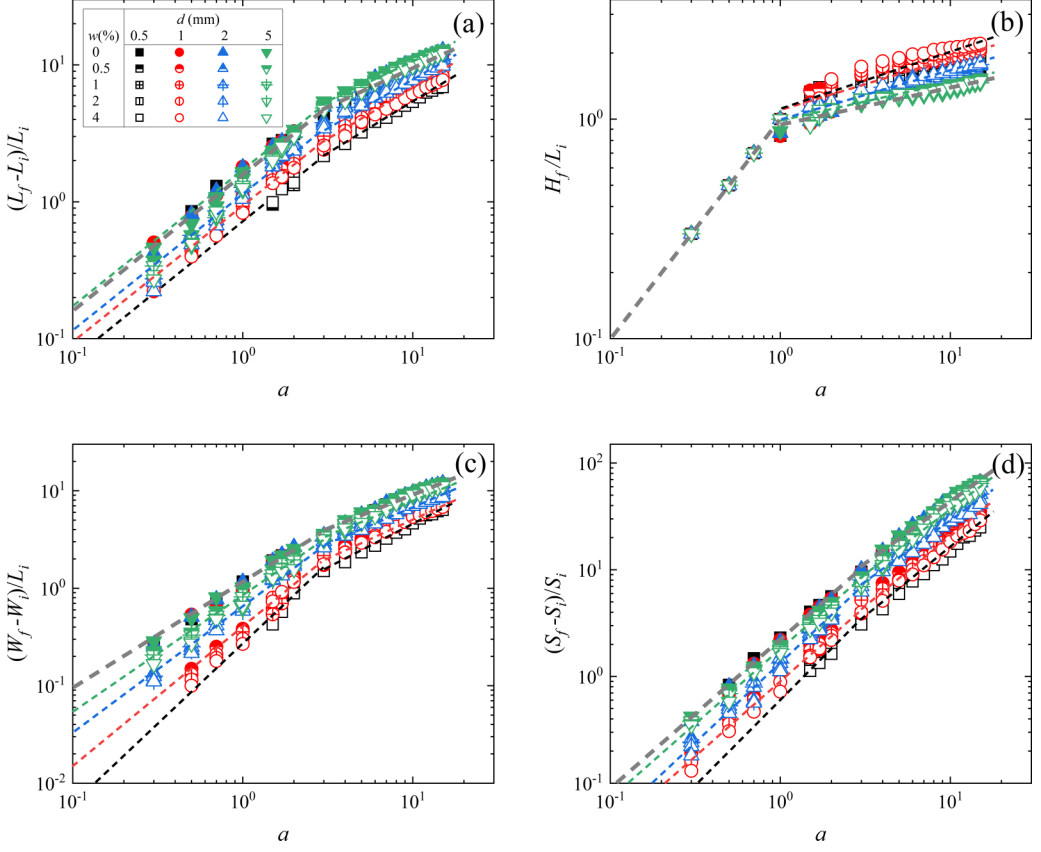
FIG. 11. The variations of normalized runout distance (a), deposit height (b), deposit width (c), and deposit area (d) with the column initial aspect ratio a for various particle sizes and water contents. The black, red, blue, and green dashed lines represent the fitted curves for wet granular materials with particle sizes of $d = 0.5, 1.0, 2.0$, and 5.0 mm, respectively, while the light gray solid lines are the fitted results for dried particles.

where the fitting coefficients A_{L1}, A_{L2}, and A_H are dependent on d and w. The exponents of scaling laws are ξ_L and ξ_H, whose values are almost independent of w and only depend on d. For comparison, these coefficients and exponents in scaling laws are summarized in Table I in the Appendix. The functional forms and corresponding critical values of a are similar to those reported for the channelized collapse of dry granular materials [43,49], but the coefficients and exponents are all related to the particle size d, which is different from the case of dry particles. Regarding the runout distance, as shown in Fig. 11(a), the values of the coefficient and exponent gradually increase with increasing d and nearly match those of dry particles at $d = 5.0$ mm. When $a > 1$, the coefficient and exponent in the scaling law for deposit height [Fig. 11(b)] decrease with increasing d and progressively approach the results for dry particles. However, if $a < 1$, the scaling law for wet particles is identical to that for dry particles. This is because the wet granular column, in this case, has also partially collapsed. It is worth noting that if d is fixed, the water content w only affects the fitting coefficients in scaling laws in a quantitative way.

To characterize the deposit region on the horizontal surface due to the spreading of wet granular material in the unchannelized configuration, the variations of normalized deposit width $(W_f - W_i)/L_i$ and deposit area $(S_f - S_i)/S_i$ with a are also presented in Figs. 11(c) and 11(d), in-

cluding the results for various water contents and particle sizes. Based on our comprehensive experimental data, these dependences likewise follow the segmental power-law functions as shown below,

$$\frac{W_f - W_i}{L_i} = \begin{cases} A_{W1}a^{\eta_{W1}} & a \geqslant 3 \\ A_{W2}a^{\eta_{W2}} & a < 3 \end{cases}, \tag{5}$$

$$\frac{S_f - S_i}{S_i} = \begin{cases} A_{S1}a^{\eta_{S1}} & a \geqslant 3 \\ A_{S2}a^{\eta_{S2}} & a < 3 \end{cases}, \tag{6}$$

where A_{W1}, A_{W2}, A_{S1}, and A_{S2} are the fitting coefficients depending on d and w. η_{W1}, η_{W2}, η_{S1}, and η_{S2} are the fitting exponents in scaling laws that are principally related to d. Similarly, Table II in the Appendix summarizes the values of coefficients and exponents for various particle sizes. The functional form of the scaling law for the deposit width well coincides with the simulation results of Girolami *et al.* [43] in an unchannelized collapse of dry particles, and the fitting exponents obtained in our experiments for dry particles as well as wet particles with larger sizes (i.e., $d = 5.0$ mm) are very close to their simulating results. It is worth noting that the dependences of coefficients and exponents on the particle size d in scaling laws for the deposit width and deposit area exhibit similar characteristics as those for the runout distance and deposit height.

The above results show that the particle size d and the water content w indeed affect the deposit morphology of wet granular material, which is directly reflected in the scaling laws that describe the dependence of morphological quantities on a. Therefore, we attempt to introduce a dimensionless parameter $B_o^{-1}w^{2/3}$ that contains both d and w as a macroscopic variable to quantify the cohesion effect at the material scale and analyze its effect on the deposit morphology of wet granular material. Here we present the variations of these morphological quantities with this dimensionless parameter at the initial aspect ratio of $a = 3$, 5, 10, and 13, respectively, as shown in Fig. 12.

These morphological quantities show similar variations with the dimensionless parameter, as seen from the plot. The results under various water contents and particle sizes all fall on the same curve for a fixed a. Using the runout distance as an example [Fig. 12(a)], the cohesion effect within the system is relatively weak when the dimensionless number $B_o^{-1}w^{2/3}$ is small, corresponding to the case of large particles, and the runout distance is extremely near to the result of dry particles, which is almost independent of the particle size. Although the runout distance shows a dependence on d and w with the increase of $B_o^{-1}w^{2/3}$, it still appears to follow a specific relationship with this dimensionless number. The experimental data for various particle sizes and water contents, including dry particles, all collapse onto the main curve that can be well described by a power function of $(L_f - L_i)/L_i \propto (B_o^{-1}w^{2/3})^{1/3}$ for a fixed a, which is consistent with that obtained in the channelized collapse of wet granular material [37]. Similarly, we find that other morphological quantities also satisfy similar power-law relationships to $B_o^{-1}w^{2/3}$ with the exponent of 1/3, and the predicted results based on these proposed scaling laws are also presented in Fig. 12 with different types of lines. This demonstrates that the dimensionless parameter $B_o^{-1}w^{2/3}$ can be regarded as the macroscopic variable that quantifies the cohesion effect of wet granular material in the pendular state.

For wet granular material, if the runout distance L_f^w is taken as an example of morphological quantities, its value tends to be the result of dry particles L_f^d when the cohesion effect within the system is weak enough, but its deviation from L_f^d becomes progressively larger as $B_o^{-1}w^{2/3}$ increases. Therefore, we examine the difference $(L_f^w - L_f^d)/L_i$ in runout distance between wet and dry particles, and find that its relative difference $(L_f^w - L_f^d)/(L_f^d - L_i)$ satisfies a power-law relationship to $B_o^{-1}w^{2/3}$ with the exponent of 1/3. More importantly, the experiment data for various a all collapse onto the main curve, showing that this relationship is no longer dependent on a. Correspondingly, other morphological quantities, including the deposit height H_f^w, the deposit width W_f^w, and the deposit area S_f^w, all show similar dependencies on $B_o^{-1}w^{2/3}$ regardless of a, as shown in Fig. 13.

As a result, by considering the cohesion effect induced by the presence of an amount of water, the morphological quantities characterizing the deposit of wet granular material can be expressed in
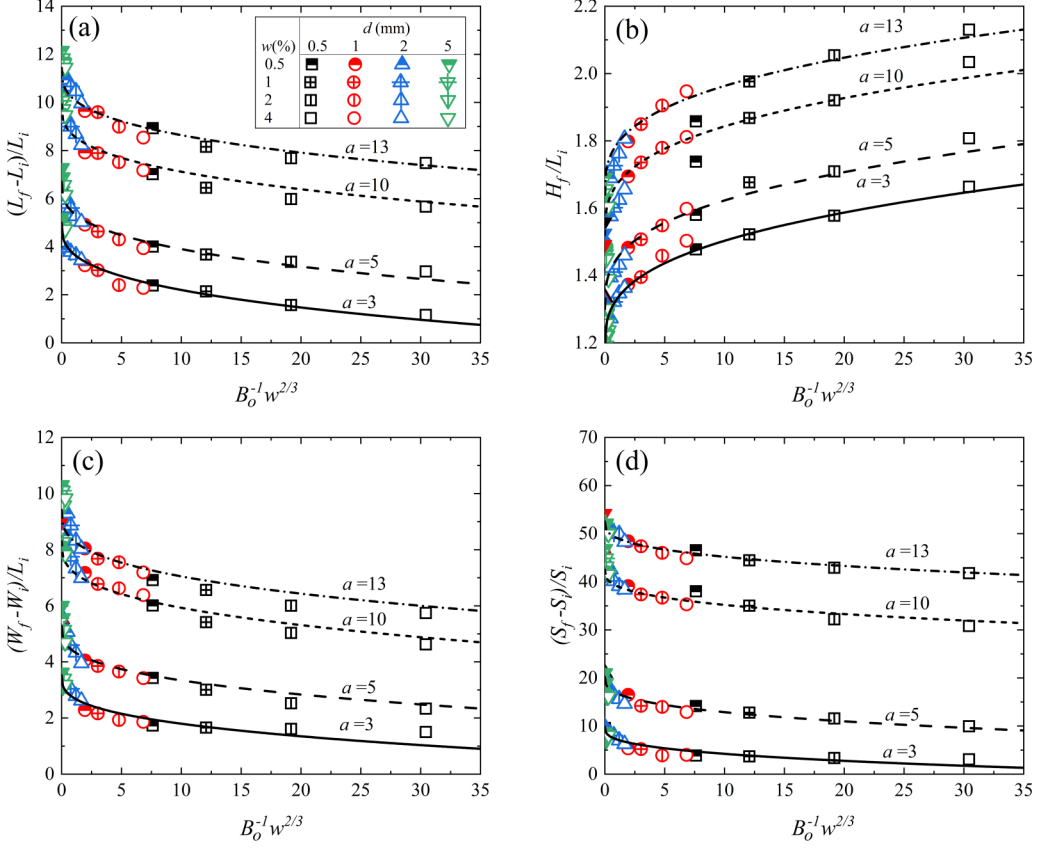
FIG. 12. Variations of normalized runout distance (a), maximum deposit height (b), deposit width (c), and deposit area (d) with the dimensionless number $B_o^{-1}w^{2/3}$ for various particle sizes and water contents at different initial aspect ratios.

terms of the corresponding results in the dry case as follows,

$$\frac{L_f^w - L_i}{L_i} = \frac{L_f^d - L_i}{L_i}\big[1 - \lambda_L\big(B_o^{-1}w^{2/3}\big)^{1/3}\big], \tag{7}$$

$$\frac{H_f^w}{L_i} = \frac{H_f^d}{L_i}\big[1 + \lambda_H\big(B_o^{-1}w^{2/3}\big)^{1/3}\big], \tag{8}$$

$$\frac{W_f^w - W_i}{L_i} = \frac{W_f^d - W_i}{L_i}\big[1 - \lambda_W\big(B_o^{-1}w^{2/3}\big)^{1/3}\big], \tag{9}$$

$$\frac{S_f^w - S_i}{S_i} = \frac{S_f^d - S_i}{S_i}\big[1 - \lambda_S\big(B_o^{-1}w^{2/3}\big)^{1/3}\big], \tag{10}$$

where $\lambda_L = 0.21$, $\lambda_H = 0.02$, $\lambda_W = 0.21$, and $\lambda_S = 0.20$ are fitting coefficients that are independent of the initial aspect ratio a, the particle size d, and the water content w. L_f^d, H_f^d, W_f^d, and S_f^d are the corresponding results of dry particles that only depend on a. Since these fitting coefficients have positive values, a minus sign in the above equations implies that the presence of the cohesion causes the corresponding morphological quantities for wet particles to decrease in comparison to that of dry particles, whereas a plus sign indicates that its value increases.

Based on scaling laws proposed in Eqs. (7)–(10), we try to rescale the relationships of morphological quantities with a in Fig. 11 by the dimensionless parameter $B_o^{-1}w^{2/3}$. For the convenience
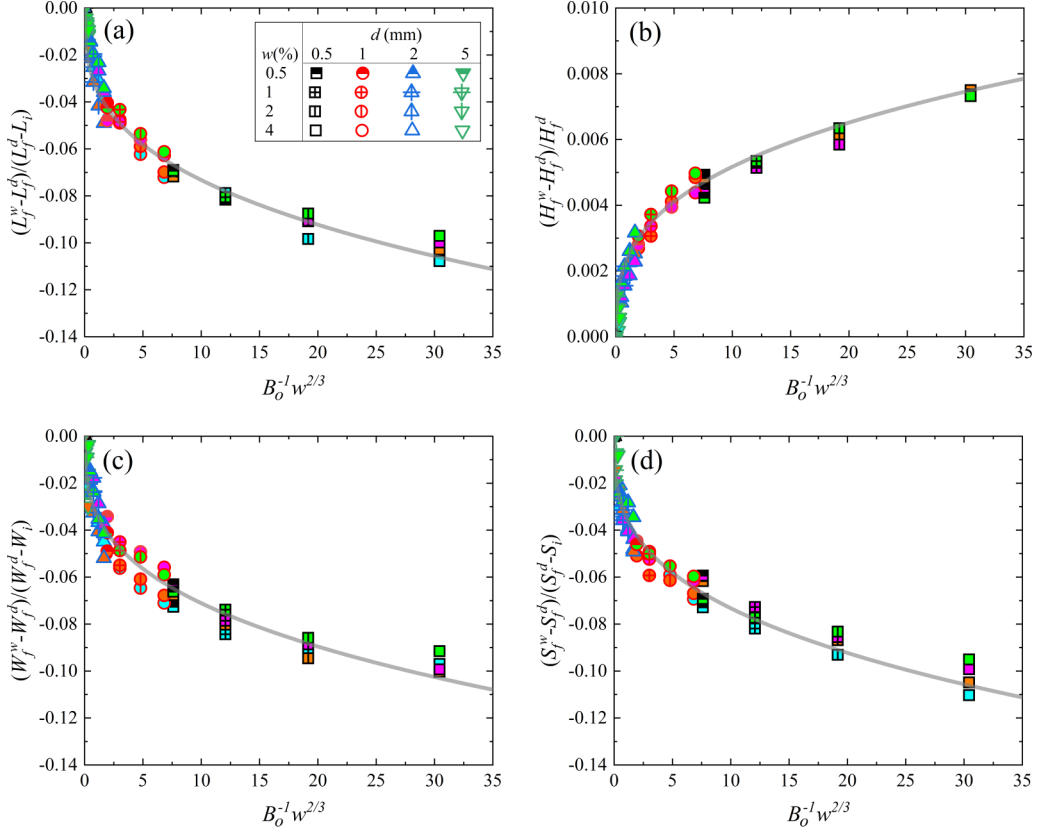
FIG. 13. Variations of the relative difference in normalized runout distance (a), deposit height (b), deposit width (c), and deposit area (d) between wet and dry particles with the dimensionless number $B_o^{-1}w^{2/3}$ for various particle sizes and water contents at different initial aspect ratios. The results for different column aspect ratios $a = 3, 5, 10,$ and 13 are filled with cyan, orange, magenta, and green, respectively. The gray curve is the fitting result based on Eqs. (7)–(10).

of description, the rescaled runout distance can be denoted by $L_f^* = \frac{(L_f - L_i)}{L_i}/[1 - \lambda_L(B_o^{-1}w^{2/3})^{1/3}]$, where L_f represents the runout distance of either dry or wet granular material. In addition to L_f, the deposit height H_f, the deposit width W_f, and the deposit area S_f can also be rescaled as H_f^*, W_f^*, and S_f^*, respectively, in a similar way, and the corresponding results are shown in Fig. 14.

As can be seen in Fig. 14, the rescaled morphological quantities are only dependent on the initial aspect ratio a after eliminating the cohesion effect induced by the particle diameter d as well as the water content w. More importantly, these relationships are consistent with the scaling laws proposed in Eqs. (3)–(6) for dry granular material, where coefficients and exponents are only dependent on a. These generalized scaling laws can be degraded to $L_f^* \propto a^{0.56}$ for $a \geqslant 3$ and $H_f^* \propto a^{0.2}$ for $a \geqslant 1$ if the cohesion effect is eliminated in the manner described above, which is well consistent with previous simulation results for dry particles in the same configuration [43]. Furthermore, for the deposit width, the proposed scaling law can also be degraded to $W_f^* \propto a^{1.1}$ for $a < 3$ and $W_f^* \propto a^{0.7}$ for $a \geqslant 3$, which is similar to the existing simulation results [43], despite the exponents being slightly different.

Overall, we have proposed the generalized scaling laws in Eqs. (7)–(10) to characterize the deposit morphology after the unchannelized collapse of a wet granular column in the pendular state, where the initial aspect ratio of the column a and the dimensionless parameter $B_o^{-1}w^{2/3}$ are two relevant variables. The latter is used to quantify the macroscopic cohesion of wet granular
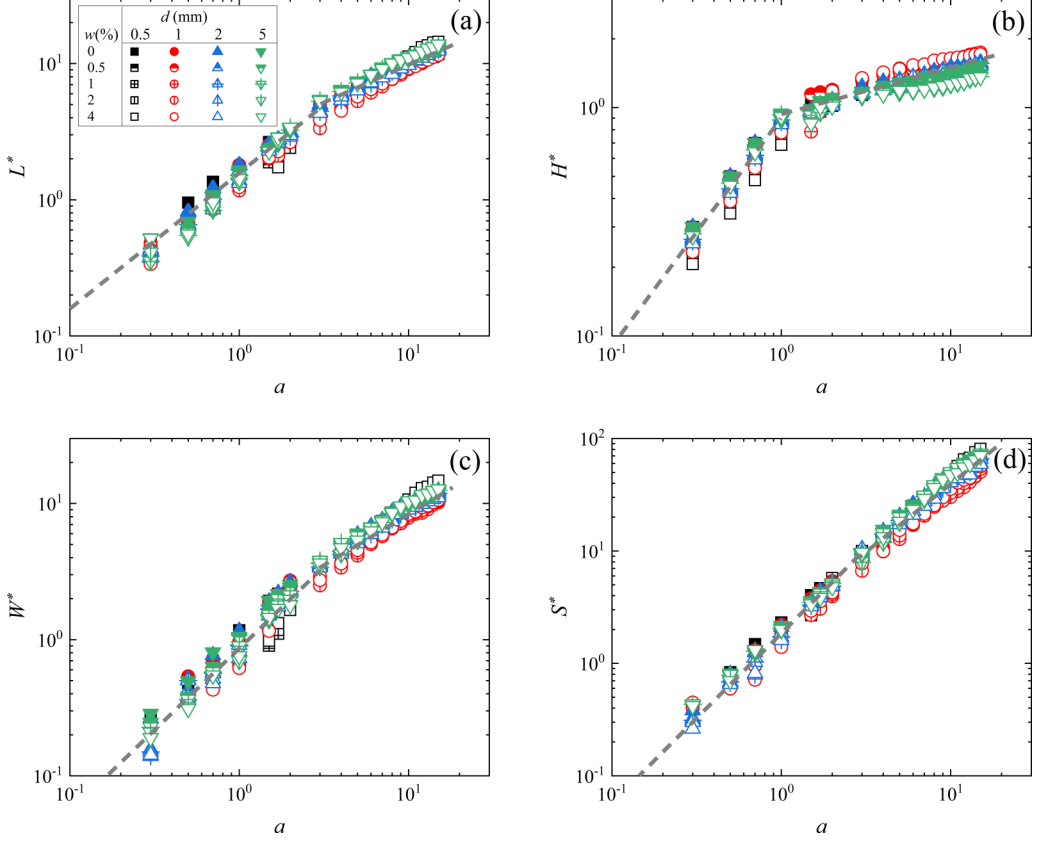
FIG. 14. Dependences of the rescaled runout distance (a), maximum deposit height (b), deposit width (c), and deposit area (d) on the initial aspect ratio a, where the light gray dashed lines represent the results predicted by the generalized scaling laws.

material. The morphological quantities in the wet case can be obtained by adding the variations due to the cohesion effect to the results of dry granular material. Correspondingly, these morphological quantities can be rescaled with the proposed dimensionless parameter, and the obtained scaling laws are suitable for describing the deposit morphology of granular materials in both wet and dry cases. When the cohesive effect within wet granular material is weak enough to be negligible, the degraded scaling laws are well consistent with those obtained in the corresponding dry granular collapse.

VI. CONCLUSIONS

In this paper, the unchannelized collapse of wet granular columns in the pendular state is investigated experimentally. Different from the unidirectional flow in a quasi-two-dimensional channel, this configuration eliminates the sidewall friction effects and more resembles mass flows in actual situations. The collapse in this configuration exhibits three different regimes, which primarily depend on the particle size d as well as the initial aspect ratio a of the column, while the water content w has a quantitative effect on the final deposit morphology. By introducing a dimensionless number $B_o^{-1} w^{2/3}$ to quantitatively characterize macroscopic cohesion within wet granular material, we propose a phase diagram in the phase space of $B_o^{-1} w^{2/3}$ and a to describe different collapse regimes of a wet granular column in an unchannelized dam-break configuration.

Furthermore, we analyze the collapse dynamics of wet granular columns and discuss its dependence on the particle size d and the initial aspect ratio a, particularly in the two regimes of collapse.

Although the flows appear to spread synchronously in both the longitudinal and lateral directions, the normalized duration of wet particles, being almost independent of a, gradually increases with d and finally converges to the result of dry granular material when d is large enough. In addition, due to the cohesion effect induced by the presence of water, the velocity field of spreading flow on the horizontal base plane exhibits different evolving characteristics in two collapse regimes, essentially resulting in the final deposit with diverse morphologies, including the height profile and the deposit shape on the horizontal surface. The lateral flow of collapsing material can be fully developed only if a is larger than a critical value, and the deposit eventually forms a nearly rounded zone on the horizontal surface even though the collapse is still in the BC regime.

Finally, generalized scaling laws have been proposed to characterize the deposit morphology after the unchannelized collapse of wet granular columns in the pendular state, with the initial aspect ratio a as well as the dimensionless parameter $B_o^{-1} w^{2/3}$ being two relevant variables considered. On this basis, the morphological quantities in the wet case may be determined by adding the amount of variations induced by the cohesion effect to the results of dry granular material. When the cohesive effect inside wet granular material is weak enough to be negligible, it has been verified that the proposed scaling laws can be well degraded to those obtained in dry granular material. This implies that these generalized scaling laws proposed in this paper can be used to characterize the deposit morphology for a broader range of granular collapse situations.

ACKNOWLEDGMENT

APPENDIX: TABLE OF FITTING PARAMETERS IN SCALING LAWS

In our experiments on the unchannelized collapse of a wet granular column in the pendular state, some scaling laws are proposed to describe the dependences of the deposit morphology on the initial aspect ratio. For the normalized runout distance and deposit height, the coefficients and exponents in the proposed scaling laws of Eqs. (3) and (4), whose values depend on the particle size, are summarized in Table I. Furthermore, for the deposit region on the horizontal surface, the dependences of normalized deposit width and deposit area on the initial aspect ratio follow the segmental power-law functions as proposed in Eqs. (5) and (6), and the values of coefficients and exponents for various particle sizes are also summarized in Table II.

TABLE I. The coefficients and exponents in scaling laws of Eqs. (3) and (4) for the runout distance and deposit height with different particle sizes.

Particle state		Runout distance		Deposit height	
		Coefficient	Exponent	Coefficient	Exponent
Dry particles		$A_{L1} = 2.84$ $A_{L2} = 1.62$	$\xi_L = 0.56$	$A_H = 0.90$	$\xi_H = 0.20$
Wet particles	0.5 mm	$A_{L1} = 0.98$ $A_{L2} = 0.72$	$\xi_L = 0.77$	$A_H = 1.15$	$\xi_H = 0.24$
	1.0 mm	$A_{L1} = 1.24$ $A_{L2} = 1.07$	$\xi_L = 0.75$	$A_H = 1.10$	$\xi_H = 0.22$
	2.0 mm	$A_{L1} = 1.88$ $A_{L2} = 1.12$	$\xi_L = 0.64$	$A_H = 1.02$	$\xi_H = 0.21$
	5.0 mm	$A_{L1} = 2.84$ $A_{L2} = 1.38$	$\xi_L = 0.56$	$A_H = 0.90$	$\xi_H = 0.20$

TABLE II. The coefficients and exponents in scaling laws of Eqs. (5) and (6) for the deposit width and deposit with different particle sizes.

Particle state		Deposit width		Deposit area	
		Coefficient	Exponent	Coefficient	Exponent
Dry particles		$A_{w1} = 1.86$	$\eta_{W1} = 0.70$	$A_{s1} = 3.20$	$\eta_{S1} = 1.30$
		$A_{w2} = 1.14$	$\eta_{W2} = 1.00$	$A_{s2} = 2.23$	$\eta_{S2} = 1.40$
Wet particles	0.5 mm	$A_{w1} = 0.58$	$\eta_{W1} = 0.90$	$A_{s1} = 0.83$	$\eta_{S1} = 1.30$
		$A_{w2} = 0.27$	$\eta_{W2} = 1.65$	$A_{s2} = 0.58$	$\eta_{S2} = 1.40$
	1.0 mm	$A_{w1} = 0.80$	$\eta_{W1} = 0.80$	$A_{s1} = 1.04$	$\eta_{S1} = 1.22$
		$A_{w2} = 0.39$	$\eta_{W2} = 1.40$	$A_{s2} = 0.92$	$\eta_{S2} = 1.30$
	2.0 mm	$A_{w1} = 1.20$	$\eta_{W1} = 0.75$	$A_{s1} = 2.03$	$\eta_{S1} = 1.25$
		$A_{w2} = 0.65$	$\eta_{W2} = 1.30$	$A_{s2} = 1.28$	$\eta_{S2} = 1.50$
	5.0 mm	$A_{w1} = 1.60$	$\eta_{W1} = 0.70$	$A_{s1} = 2.62$	$\eta_{S1} = 1.28$
		$A_{w2} = 0.85$	$\eta_{W2} = 1.20$	$A_{s2} = 1.87$	$\eta_{S2} = 1.34$

[1] R. M. Iverson, The physics of debris flows, Rev. Geophys. 35, 245 (1997).

[2] N. J. Balmforth and R. R. Kerswell, Granular collapse in two dimensions, J. Fluid Mech. 538, 399 (2005).

[3] G. G. D. Zhou, D. Song, C. E. Choi, A. Pasuto, Q. C. Sun, and D. F. Dai, Surge impact behavior of granular flows: Effects of water content, Landslides 15, 695 (2017).

[4] A. V. R. Delannay, A. Mangeney, O. Roche, and P. Richard, Granular and particle-laden flows: From laboratory experiments to field observations, J. Phys. D: Appl. Phys. 50, 053001 (2017).

[5] G. Lube, H. E. Huppert, R. S. J. Sparks, and A. Freundt, Static and flowing regions in granular collapses down channels, Phys. Fluids 19, 043301 (2007).

[6] L. Rondon, O. Pouliquen, and P. Aussillous, Granular collapse in a fluid: Role of the initial volume fraction, Phys. Fluids 23, 073301 (2011).

[7] V. Topin, Y. Monerie, F. Perales, and F. Radjai, Collapse Dynamics and Runout of Dense Granular Materials in a Fluid, Phys. Rev. Lett. 109, 188001 (2012).

[8] C. Mériaux and T. Triantafillou, Scaling the final deposits of dry cohesive granular columns after collapse and quasi-static fall, Phys. Fluids 20, 033301 (2008).

[9] V. J. Langlois, A. Quiquerez, and P. Allemand, Collapse of a two-dimensional brittle granular column: Implications for understanding dynamic rock fragmentation in a landslide, J. Geophys. Res.: Earth Surf. 120, 1866 (2015).

[10] K. L. Johnson, K. Kendall, and A. D. Roberts, Surface energy and the contact of elastic solids, Proc. R. Soc. London, Ser. A 324, 301 (1971).

[11] A. Hemmerle, M. Schröter, and L. Goehring, A cohesive granular material with tunable elasticity, Sci. Rep. 6, 35650 (2016).

[12] F. Gabrieli, P. Lambert, S. Cola, and F. Calvetti, Micromechanical modelling of erosion due to evaporation in a partially wet granular slope, Int. J. Numer. Anal. Methods Geomech. 36, 918 (2012).

[13] S. M. Iveson, J. D. Litster, K. Hapgood, and B. J. Ennis, Nucleation, growth and breakage phenomena in agitated wet granulation processes: A review, Powder Technol. 117, 3 (2001).

[14] N. Mitarai and F. Nori, Wet granular materials, Adv. Phys. 55, 1 (2007).

[15] G. Wang, A. Riaz, and B. Balachandran, Smooth particle hydrodynamics studies of wet granular column collapses, Acta Geotech. 15, 1205 (2019).

[16] J.-P. Wang, X. Li, and H.-S. Yu, A micro-macro investigation of the capillary strengthening effect in wet granular materials, Acta Geotech. 13, 513 (2017).

[17] S. Roy, Hydrodynamic theory of wet particle systems, Ph.D. thesis, The University of Twente, 2018.

[18] V. D. Than, S. Khamseh, A. M. Tang, J.-M. Pereira, F. Chevoir, and J.-N. Roux, Basic mechanical properties of wet granular materials: A DEM study, J. Eng. Mech. **143**, C4016001 (2017).

[19] B. Mohan, C. Kloss, J. Khinast, and S. Radl, Regimes of liquid transport through sheared beds of inertial smooth particles, Powder Technol. **264**, 377 (2014).

[20] D. J. Hornbaker, R. Albert, I. Albert, A. L. Barabasi, and P. Schiffer, What keeps sandcastles standing? Nature (London) **387**, 765 (1997).

[21] S. Nowak, A. Samadani, and A. Kudrolli, Maximum angle of stability of a wet granular pile, Nat. Phys. **1**, 50 (2005).

[22] V. Richefeu, M. S. El Youssoufi, and F. Radjai, Shear strength properties of wet granular materials, Phys. Rev. E **73**, 051304 (2006).

[23] P. C. F. Møller and D. Bonn, The shear modulus of wet granular matter, EPL **80**, 38002 (2007).

[24] M. Scheel, R. Seemann, M. Brinkmann, M. Di Michiel, A. Sheppard, and S. Herminghaus, Liquid distribution and cohesion in wet granular assemblies beyond the capillary bridge regime, J. Phys.: Condens. Matter **20**, 494236 (2008).

[25] H. Shi, S. Roy, T. Weinhart, V. Magnanimo, and S. Luding, Steady state rheology of homogeneous and inhomogeneous cohesive granular materials, Granular Matter **22**, 14 (2019).

[26] B. Remy, J. G. Khinast, and B. J. Glasser, Wet granular flows in a bladed mixer: Experiments and simulations of monodisperse spheres, AIChE J. **58**, 3354 (2012).

[27] D. J. Koeze and B. P. Tighe, Sticky Matters: Jamming and Rigid Cluster Statistics with Attractive Particle Interactions, Phys. Rev. Lett. **121**, 188002 (2018).

[28] P. Tegzes, T. Vicsek, and P. Schiffer, Development of correlations in the dynamics of wet granular avalanches, Phys. Rev. E **67**, 051303 (2003).

[29] P. Y. Liu, R. Y. Yang, and A. B. Yu, Dynamics of wet particles in rotating drums: Effect of liquid surface tension, Phys. Fluids **23**, 013304 (2011).

[30] A. Jarray, V. Magnanimo, and S. Luding, Wet granular flow control through liquid induced cohesion, Powder Technol. **341**, 126 (2019).

[31] L. Lacaze, J. C. Phillips, and R. R. Kerswell, Planar collapse of a granular column: Experiments and discrete element simulations, Phys. Fluids **20**, 063302 (2008).

[32] E. Lajeunesse, A. Mangeney-Castelnau, and J. P. Vilotte, Spreading of a granular mass on a horizontal plane, Phys. Fluids **16**, 2371 (2004).

[33] O. Roche, M. Attali, A. Mangeney, and A. Lucas, On the run-out distance of geophysical gravitational flows: Insight from fluidized granular collapse experiments, Earth Planet. Sci. Lett. **311**, 375 (2011).

[34] G. Lube, H. E. Huppert, R. S. J. Sparks, and M. A. Hallworth, Axisymmetric collapses of granular columns, J. Fluid Mech. **508**, 175 (2004).

[35] G. Lube, H. E. Huppert, R. S. Sparks, and A. Freundt, Collapses of two-dimensional granular columns, Phys. Rev. E **72**, 041301 (2005).

[36] Y. Wu, P. Li, and D. Wang, Erosion-deposition regime formation in granular column collapse over an erodible surface, Phys. Rev. E **98**, 052909 (2018).

[37] R. Artoni, A. C. Santomaso, F. Gabrieli, D. Tono, and S. Cola, Collapse of quasi-two-dimensional wet granular columns, Phys. Rev. E **87**, 032205 (2013).

[38] F. Gabrieli, R. Artoni, A. Santomaso, and S. Cola, Discrete particle simulations and experiments on the collapse of wet granular columns, Phys. Fluids **25**, 103303 (2013).

[39] A. C. Santomaso, S. Volpato, and F. Gabrieli, Collapse and runout of granular columns in pendular state, Phys. Fluids **30**, 063301 (2018).

[40] A. Abramian, P. Y. Lagree, and L. Staron, How cohesion controls the roughness of a granular deposit, Soft Matter **17**, 10723 (2021).

[41] P. Li, D. Wang, Y. Wu, and Z. Niu, Experimental study on the collapse of wet granular column in the pendular state, Powder Technol. **393**, 357 (2021).

[42] Y. Zhou, B. Wright, R. Yang, B. Xu, and A. Yu, Rolling friction in the dynamic simulation of sandpile formation, Physica A **269**, 536 (1999).

[43] L. Girolami, A. Wachs, and G. Vinay, Unchannelized dam-break flows: Effects of the lateral spreading on the flow dynamics, Phys. Fluids **25**, 043306 (2013).

[44] L. Staron and E. Hinch, Study of the collapse of granular columns using two-dimensional discrete-grain simulation, J. Fluid Mech. **545**, 1 (2005).

[45] W. Sarlin, C. Morize, A. Sauret, and P. Gondret, Collapse dynamics of dry granular columns: From free-fall to quasistatic flow, Phys. Rev. E **104**, 064904 (2021).

[46] H. Xiao, J. Hruska, J. M. Ottino, R. M. Lueptow, and P. B. Umbanhowar, Unsteady flows and inhomogeneous packing in damp granular heap flows, Phys. Rev. E **98**, 032906 (2018).

[47] L. Sarno, A. Carravetta, Y.-C. Tai, R. Martino, M. N. Papa, and C.-Y. Kuo, Measuring the velocity fields of granular flows—employment of a multi-pass two-dimensional particle image velocimetry (2D-PIV) approach, Adv. Powder Technol. **29**, 3107 (2018).

[48] B. Huang, J. Wang, Q. Zhang, C. Luo, and X. Chen, Energy conversion and deposition behaviour in gravitational collapse of granular columns, J. Mt. Sci. **17**, 216 (2020).

[49] C. Lee, Z. Huang, and Y. Chiew, A three-dimensional continuum model incorporating static and kinetic effects for granular flows with applications to collapse of a two-dimensional granular column, Phys. Fluids **27**, 113303 (2015).

[50] E. Lajeunesse, J. B. Monnier, and G. M. Homsy, Granular slumping on a horizontal surface, Phys. Fluids **17**, 103302 (2005).

[51] Y. Wu, D. Wang, and P. Li, The collapse of a granular column onto an erodible bed: Dynamics and morphology scaling, Granular Matter **23**, 31 (2021).